A PROJECT REPORT

on

INVESTIGATION OF SNAP-THROUGH PHENOMENON IN THIN SHALLOW ARCH USING COROTATIONAL FINITE ELEMENT FORMULATION

for the course of

CE622A Stability of Structures

by

RUPSAGAR CHATTERJEE (20103098)

done under the guidance of

PROFESSOR AMAR NATH ROY CHOWDHURY

IIT Kanpur

Civil Engineering Department

Date of submission: 16/05/2021

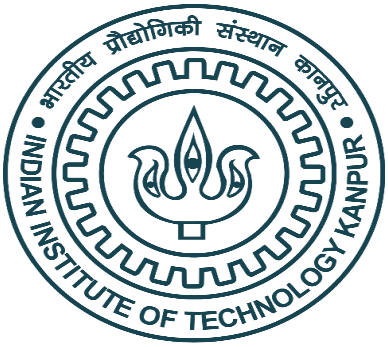

CIVIL ENGINEERING DEPARTMENT

INDIAN INSTITUTE OF TECHNOLOGY KANPUR

KANPUR 208016

Investigation of snap-through phenomenon in thin shallow arch using corotational finite element formulation

1. Problem Statement

Different engineering fields require the use of thin shallow arch like structure. Arches which have very low value of height to span ratio as well as thickness to span ratio are generally classified as thin shallow arches. These structures under the application of a critical load undergoes snap-through phenomenon. After loading the structure beyond the critical load, when it is unloaded, the structure follows a different equilibrium path. Hence the structure shows a hysteretic behaviour when subjected to an arbitrary load-displacement history. Since the structure shows a snap-through phenomenon, the load-displacement curve cannot be traced using a load-controlled analysis. Instead displacement-controlled analysis or analysis where load and displacement are controlled simultaneously needs to be done to trace the snap-through phenomenon.

In the present study, the load displacement behaviour of a thin shallow arch structure with linear elastic material is studied using corotational finite element models using displacement-controlled algorithm. Two methods of discretization are adopted in this study. In one case, the geometry of the thin shallow arch is discretized using corotational truss elements. This approach of discretization was followed by Xenidis et al. 2013. The results obtained from the present study are matched with that obtained by Xenidis et al. 2013. In the second case, the geometry is discretized using corotational beam elements and the results are compared with that obtained from the first case. Only geometric nonlinearities are considered in this study with no consideration of material nonlinearities.

For the purpose of implementing the corotational truss and beam finite element formulations and the displacement-controlled algorithm, in house MATLAB codes are written which are validated from the works of Yaw 2009 and Vasios 2015. A Newton-Raphson iterative algorithm is adopted for the structural convergence. The convergence criterion is taken as energy increment due to unbalanced generalized force. The choice of energy increment as the convergence criterion provides an advantage since the generalized forces contain both forces and moments and generalized displacements contain both displacements and rotations for the beam element. The tolerance criterion is kept as 10^{-16} with a maximum of 10 iterations allowed for all cases.

2. Solution Methodology

2.1. Corotational truss finite element formulation

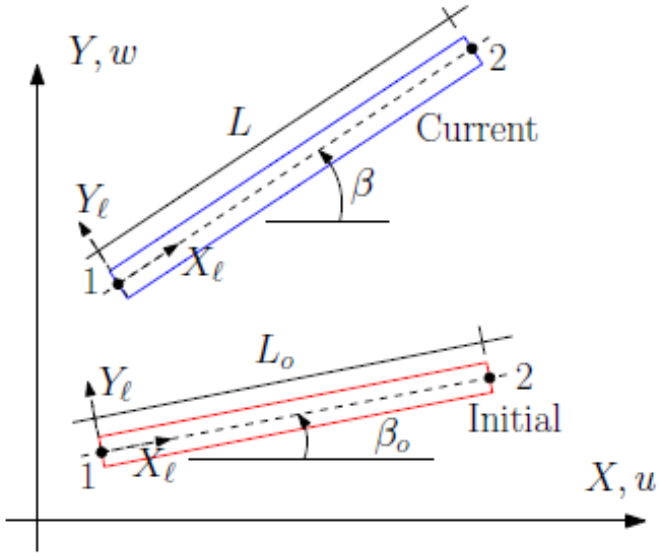

Figure 1: Initial and current configuration of truss element (Yaw 2009)

In corotational formulation, the rigid body modes namely rotation and translation of an element are separated out by attaching a local reference frame to the element to obtain the deformations causing internal forces in the element.

In Figure 1 (Yaw 2009), a truss element is shown in initial and final configuration. The original and final lengths of the element in both configurations are given as,

$$L_0 = \sqrt{(X_2 - X_1)^2 + (Y_2 - Y_1)^2} \qquad (1)$$

$$L = \sqrt{((X_2 + u_2) - (X_1 + u_1))^2 + ((Y_2 + w_2) - (Y_1 + w_1))^2} \qquad (2)$$

The change of length of the element along the local X axis is given as,

$$u_l = L - L_0 \qquad (3)$$

The axial force in the element is given by,

$$N = \frac{EAu_l}{L_0} \qquad (4)$$

The cosine and sine of the current angle of the corotating frame with respect to the global axis are given as,

$$cos\,\beta = \frac{(X_2+u_2)-(X_1+u_1)}{L} \qquad (5) \qquad sin\,\beta = \frac{(Y_2+w_2)-(Y_1+w_1)}{L} \qquad (6)$$

For simplicity in representation let,

$$c = cos\,\beta \qquad (7) \qquad s = sin\,\beta \qquad (8)$$

The internal forces of the truss element in the local coordinate system is given as,

$$\mathbf{q_l} = [-N \quad 0 \quad N \quad 0]^T \qquad (9)$$

The global internal force vector of the element is given as,

$$\mathbf{q} = \mathbf{T}^T \mathbf{q_l} \qquad (10)$$

where,

$$\mathbf{T} = \begin{bmatrix} c & s & 0 & 0 \\ -s & c & 0 & 0 \\ 0 & 0 & c & s \\ 0 & 0 & -s & c \end{bmatrix} \qquad (11)$$

is the transformation matrix from the local coordinate to the global coordinate system.

From the principle of virtual work, the material stiffness matrix for truss element in local coordinate system is given as,

$$\mathbf{k_M} = \frac{AE}{L_0} \begin{bmatrix} 1 & 0 & -1 & 0 \\ 0 & 0 & 0 & 0 \\ -1 & 0 & 1 & 0 \\ 0 & 0 & 0 & 0 \end{bmatrix} \qquad (12)$$

Similarly, the geometric stiffness matrix in the local system for large strain condition is given as,

$$\mathbf{k_G} = \frac{N}{L} \begin{bmatrix} 1 & 0 & -1 & 0 \\ 0 & 1 & 0 & -1 \\ -1 & 0 & 1 & 0 \\ 0 & -1 & 0 & 1 \end{bmatrix} \qquad (13)$$

whereas for small strain condition, the geometric stiffness matrix is given as,

$$\mathbf{k_G} = \frac{N}{L} \begin{bmatrix} 0 & 0 & 0 & 0 \\ 0 & 1 & 0 & -1 \\ 0 & 0 & 0 & 0 \\ 0 & -1 & 0 & 1 \end{bmatrix} \qquad (14)$$

In the present study, the geometric stiffness matrix corresponding to large strain condition is taken. Finally, the tangent stiffness matrix of the truss element in the global system is given as,

$$\mathbf{K_T} = \mathbf{T}^T(\mathbf{k_M} + \mathbf{k_G})\mathbf{T} \qquad (15)$$

The global force vectors and the global tangent stiffness matrices of the different elements are assembled in the appropriate degrees of freedom (DOFs) of the structure to obtain the structural internal resisting force vector and the total structural stiffness matrix at any iteration step in the solution algorithm. Finally, the structural boundary conditions are imposed on the assembled system stiffness matrix and system internal force vector to obtain the structural stiffness matrix and the resisting force vector in the unrestrained DOFs.

2.2. Corotational beam finite element formulation

In the corotational beam formulation, the beam element along with rigid rotation and axial stretching also undergoes flexural deformation. The analysis of the element involves the same concept of elimination of the rigid body modes using the corotating local axis to obtain the displacements causing internal forces in the element as followed in the case of truss element. The determination of the axial forces and strain as well as the cosine and sine of current orientation of the local coordinate system of the beam element are same as that for a corotational truss element (equations 1 to 8).

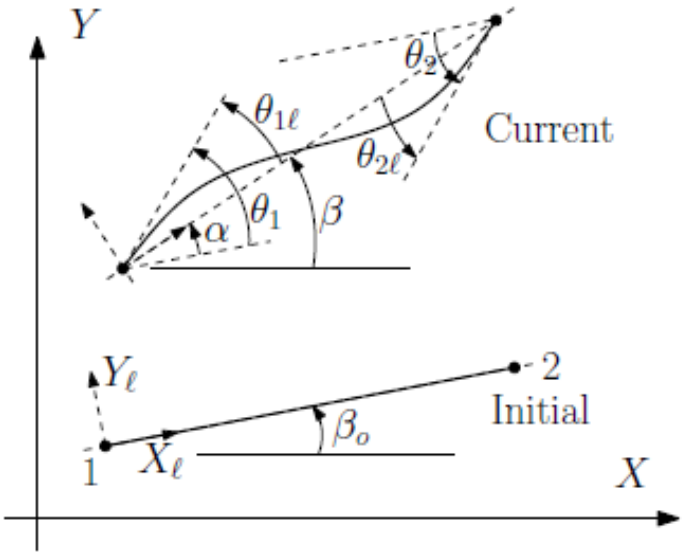

Figure 2: Initial and current configuration of beam element (Yaw 2009)

In Figure 2 (Yaw 2009), a beam element is shown with the flexural deformations. The local nodal rotations are given by,

$$\theta_{1l} = \theta_1 + \beta_0 - \beta \qquad (16) \qquad \theta_{2l} = \theta_2 + \beta_0 - \beta \qquad (17)$$

where, θ_1,θ_2 are the nodal rotations obtained from global system equations.

The initial and current angle of the element with the global coordinate is obtained as follows,

$$\beta_0 = tan^{-1}\left(\frac{Y_2 - Y_1}{X_2 - X_1}\right) \qquad (18) \qquad \beta = tan^{-1}\left(\frac{(Y_2 + w_2) - (Y_1 + w_1)}{(X_2 + u_2) - (X_1 + u_1)}\right) \qquad (19)$$

The local rotations can be obtained as,

$$\theta_{1l} = tan^{-1}\left(\frac{cos\,\beta\, sin\,\beta_1 - sin\,\beta\, cos\,\beta_1}{cos\,\beta\, cos\,\beta_1 + sin\,\beta\, sin\,\beta_1}\right) \qquad (20)$$

$$\theta_{2l} = tan^{-1}\left(\frac{cos\,\beta\, sin\,\beta_2 - sin\,\beta\, cos\,\beta_2}{cos\,\beta\, cos\,\beta_2 + sin\,\beta\, sin\,\beta_2}\right) \qquad (21)$$

where, the new variables are defined as,

$$\beta_1 = \theta_1 + \beta_0 \qquad (22) \qquad \beta_2 = \theta_2 + \beta_0 \qquad (23)$$

Therefore, the generalized forces in the element in the local system can be written as follows,

$$\begin{bmatrix} N \\ M_1 \\ M_2 \end{bmatrix} = \begin{bmatrix} \frac{EA}{L_0} & 0 & 0 \\ 0 & \frac{4EI}{L_0} & \frac{2EI}{L_0} \\ 0 & \frac{2EI}{L_0} & \frac{4EI}{L_0} \end{bmatrix} \begin{bmatrix} u_l \\ \theta_{1l} \\ \theta_{2l} \end{bmatrix} \Rightarrow \mathbf{q_l} = \mathbf{C_l p_l} \qquad (24)$$

2.2.1. Derivation of corotational beam stiffness matrix

A relationship is established between the local and global nodal displacements considering the stretching of the element in the local axis and its rigid rotation.

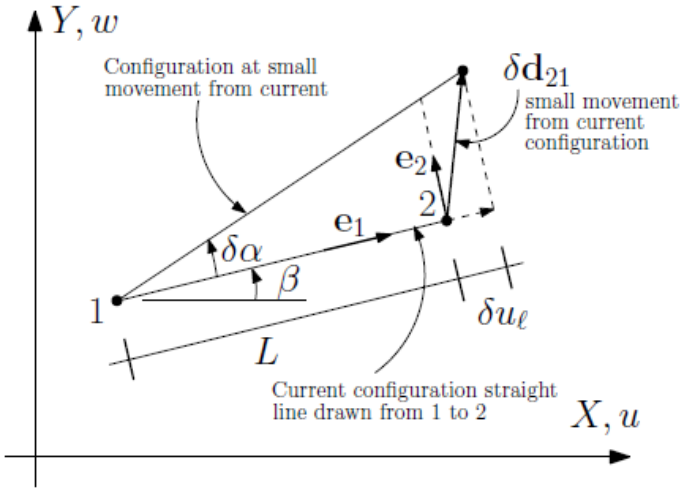

Figure 3: Element subjected to virtual displacement and rigid rotation (Yaw 2009)

In Figure 3 (Yaw 2009), a small virtual displacement is given from the current configuration of the element.

$$\delta u_l = \mathbf{e}_1{}^T \delta \mathbf{d}_{21} = \begin{bmatrix} cos\,\beta \\ sin\,\beta \end{bmatrix}^T \delta \mathbf{d}_{21} \qquad (25)$$

where,

$$\delta \mathbf{d}_{21} = \begin{bmatrix} \delta u_2 - \delta u_1 \\ \delta w_2 - \delta w_1 \end{bmatrix} \qquad (26)$$

is the difference in the incremental displacement at the two ends. Simplifying,

$$\delta u_l = [-c \quad -s \quad 0 \quad c \quad s \quad 0]\delta \mathbf{p} = \boldsymbol{r}^T \delta \boldsymbol{p} \qquad (27)$$

where,

$$\mathbf{p} = [u_1 \quad w_1 \quad \theta_1 \quad u_2 \quad w_2 \quad \theta_2]^T \qquad (28)$$

is the global nodal displacement vector.

The variational rigid rotation can be written as,

$$\delta\alpha = \frac{1}{L}\mathbf{e}_2{}^T \delta \mathbf{d}_{21} = \begin{bmatrix} -\,sin\,\beta \\ cos\,\beta \end{bmatrix}^T \delta \mathbf{d}_{21} \qquad (29)$$

which can be simplified to write,

$$\delta\alpha = \frac{1}{L}[s \quad -c \quad 0 \quad -s \quad c \quad 0]\delta \mathbf{p} = \frac{1}{L}\mathbf{z}^T \delta \mathbf{p} \qquad (30)$$

Now the variation in local rotations is given as,

$$\delta \boldsymbol{\theta}_\mathbf{l} = \delta \begin{bmatrix} \theta_1 + \beta_0 - \beta \\ \theta_2 + \beta_0 - \beta \end{bmatrix} = \begin{bmatrix} \delta\theta_1 + \delta\beta_0 - \delta\beta \\ \delta\theta_2 + \delta\beta_0 - \delta\beta \end{bmatrix} = \begin{bmatrix} \delta\theta_1 - \delta\alpha \\ \delta\theta_2 - \delta\alpha \end{bmatrix} \qquad (31)$$

where,

$$\delta\beta_0 = 0 \qquad (32) \qquad\qquad \delta\beta = \delta\alpha \qquad (33)$$

After simplification $\delta \boldsymbol{\theta}_\mathbf{l}$ can be written as,

$$\delta \boldsymbol{\theta}_\mathbf{l} = \left[\begin{bmatrix} 0 & 0 & 1 & 0 & 0 & 0 \\ 0 & 0 & 0 & 0 & 0 & 1 \end{bmatrix} - \frac{1}{L}\begin{bmatrix} \mathbf{z}^T \\ \mathbf{z}^T \end{bmatrix} \right] \delta \mathbf{p} = \mathbf{A}^T \delta \mathbf{p} \qquad (34)$$

Therefore, the relation between the infinitesimal local and global displacements are given as,

$$\delta \mathbf{p_l} = \begin{bmatrix} \delta u_l \\ \delta \theta_{1l} \\ \delta \theta_{2l} \end{bmatrix} = \begin{bmatrix} \mathbf{r}^T \\ \mathbf{A}^T \end{bmatrix} \delta \mathbf{p} = \mathbf{B} \delta \mathbf{p} \qquad (35)$$

where, the transformation matrix is given as,

$$\boldsymbol{B} = \begin{bmatrix} -c & -s & 0 & c & s & 0 \\ -s/L & c/L & 1 & s/L & -c/L & 0 \\ -s/L & c/L & 0 & s/L & -c/L & 1 \end{bmatrix} \qquad (36)$$

From the principle of equivalence of virtual work in global and local coordinate,

$$\delta \mathbf{p}^T \mathbf{q} = \delta \mathbf{p_l}^T \mathbf{q_l} \qquad (37)$$

where, the subscript l denotes the local system quantities.

Substituting from the relation of incremental displacement between global and local system,

$$\delta \mathbf{p}^T \mathbf{q} = (\mathbf{B} \delta \mathbf{p})^T \mathbf{q_l} = \delta \mathbf{p}^T \mathbf{B}^T \mathbf{q_l} \qquad (38)$$

Since this is true for any arbitrary variation $\delta \mathbf{p}$,

$$\mathbf{q} = \mathbf{B}^T \mathbf{q_l} \qquad (39)$$

which, gives the relation between local and global element forces.

Taking variation of equation 39,

$$\delta \mathbf{q} = \mathbf{B}^T \delta \mathbf{q_l} + \delta \mathbf{B}^T \mathbf{q_l} = \mathbf{B}^T \delta \mathbf{q_l} + N \delta \mathbf{B_1} + M_1 \delta \mathbf{B_2} + M_2 \delta \mathbf{B_3} \qquad (40)$$

$$\delta \mathbf{q} = \boldsymbol{K_M} \delta \mathbf{p} + \boldsymbol{K_G} \delta \mathbf{p} \qquad (41)$$

where, $\boldsymbol{B_1}, \boldsymbol{B_2}, \boldsymbol{B_3}$ are the first, second and third column of $\boldsymbol{B}^T$. $\mathbf{K_M}$ and $\mathbf{K_G}$ are the material and geometric stiffness matrix respectively in the global coordinate system. From equation 24,

$$\delta \boldsymbol{q}_l = \boldsymbol{C}_l \delta \boldsymbol{p}_l \qquad (42)$$

Therefore,

$$\mathbf{B}^T \delta \mathbf{q_l} = \mathbf{B}^T \mathbf{C_l} \delta \mathbf{p_l} = \mathbf{B}^T \mathbf{C_l} \mathbf{B} \delta \mathbf{p} \qquad (43)$$

and,

$$\boldsymbol{K_M} = \mathbf{B}^T \mathbf{C_l} \mathbf{B} \qquad (44)$$

which gives the material stiffness matrix in the global coordinate for the 2D beam element.

For the geometric stiffness matrix, variation of each of the columns of $\boldsymbol{B}^T$ needs to be taken. The variation of the first column yields,

$$\delta \boldsymbol{B_1} = \delta \mathbf{r} = \delta [-c \quad -s \quad 0 \quad c \quad s \quad 0]^T = [s \quad -c \quad 0 \quad -s \quad c \quad 0]^T \delta \beta = \mathbf{z} \delta \beta \qquad (45)$$

Further simplification using equations 30 and 33 gives the following,

$$\delta \mathbf{B_1} = \frac{1}{L} \mathbf{z} \mathbf{z}^T \delta \mathbf{p} \qquad (46)$$

The variation of the second column of $\boldsymbol{B}^T$ yields,

$$\delta \mathbf{B_2} = \delta \left(-\frac{\mathbf{z}}{L} \right) = \mathbf{z} \delta \left(-\frac{1}{L} \right) + \left(-\frac{1}{L} \right) \delta \mathbf{z} \qquad (47)$$

The variation of the two terms are found separately. The first term gives,

$$\delta\left(-\frac{1}{L}\right) = \frac{1}{L^2}\delta L = \frac{1}{L^2}\delta(L_0 + u_l) = \frac{1}{L^2}\delta u_l = \frac{1}{L^2}\mathbf{r}^T\delta\mathbf{p} \qquad (48)$$

The second term gives,

$$\delta\mathbf{z} = \delta[s \quad -c \quad 0 \quad -s \quad c \quad 0]^T = [c \quad s \quad 0 \quad -c \quad -s \quad 0]^T\delta\beta = -\frac{1}{L}\mathbf{r}\mathbf{z}^T\delta\mathbf{p} \qquad (49)$$

Substituting the values from equations 48 and 49 into equation 47 gives,

$$\delta\mathbf{B_2} = \frac{1}{L^2}\mathbf{z}\mathbf{r}^T\delta\mathbf{p} + \frac{1}{L^2}\mathbf{r}\mathbf{z}^T\delta\mathbf{p} = \frac{1}{L^2}(\mathbf{z}\mathbf{r}^T + \mathbf{r}\mathbf{z}^T)\delta\mathbf{p} \qquad (50)$$

Also, it can be seen,

$$\delta\mathbf{B_3} = \delta\mathbf{B_2} \qquad (51)$$

Substituting the variation of $\boldsymbol{B_1}$, $\boldsymbol{B_2}$, $\boldsymbol{B_3}$, gives the geometric stiffness matrix as,

$$\mathbf{K_G} = \frac{N}{L}\mathbf{z}\mathbf{z}^T + \frac{M_1+M_2}{L^2}(\mathbf{z}\mathbf{r}^T + \mathbf{r}\mathbf{z}^T) \qquad (52)$$

Therefore, the element tangent stiffness matrix is written as (de Borst et al. 2012, Yaw 2009),

$$\mathbf{K_T} = \mathbf{K_M} + \mathbf{K_G} = \mathbf{B}^T\mathbf{C_l}\mathbf{B} + \frac{N}{L}\mathbf{z}\mathbf{z}^T + \frac{M_1+M_2}{L^2}(\mathbf{z}\mathbf{r}^T + \mathbf{r}\mathbf{z}^T) \qquad (53)$$

The first term in the tangent stiffness constitutes the material stiffness while the last two term arises due to the geometric stiffness of the element.

As in the case of truss element, the global force vectors and the global tangent stiffness matrices of the different beam elements are assembled in the appropriate DOFs of the structure to obtain the structural internal resisting force vector and the total structural stiffness matrix at any iteration step in the solution algorithm. Finally, the structural boundary conditions are imposed on the assembled system stiffness matrix and system internal force vector to obtain the structural stiffness matrix and the resisting force vector in the unrestrained DOFs.

2.3. Formulation of displacement control algorithm

In a displacement control analysis. the displacement in a particular degree of freedom (DOF) at a particular node is increased in a controlled manner as the displacements at other nodes are found iteratively till the internal resisting forces balance the external loads (Ramm 1981).

At any iteration step *j*, the equilibrium equation between the external applied loads and the unbalanced loads is given as,

$$\mathbf{K}\Delta\mathbf{r}^j = \Delta\lambda^j\mathbf{R_{ref}} + \mathbf{R_U^j} \qquad (54)$$

Equation 54 can be simplified to obtain nodal displacements as,

$$\Delta\mathbf{r}^j = \Delta\lambda^j\Delta\mathbf{r_I^j} + \Delta\mathbf{r_{II}^j} \qquad (55)$$

Let *k* be the DOF where the displacement is controlled. Then the linear equation in k^{th} DOF becomes,

$$\Delta r_k^j = \Delta\lambda^j\Delta r_{I,k}^j + \Delta r_{II,k}^j \qquad (56)$$

For the first iteration, the known displacement is applied at the k^{th} DOF,

$$\Delta r_k^1 = \Delta\hat{r} \qquad (57)$$

The incremental load factor in the first iteration is,

$$\Delta\lambda^1 = \frac{\Delta\hat{r}}{\Delta r_{I,k}^1} \qquad (58)$$

whereas for all subsequent iterations, the incremental load factor is given by,

$$\Delta\lambda^j = \frac{\Delta r_{II,k}^j}{\Delta r_{I,k}^j} \qquad (59)$$

The cumulative load factor at any displacement control step n is updated after every iteration as follows,

$$\Delta\lambda_n = \Delta\lambda_n + \Delta\lambda^j \qquad (60)$$

with $\Delta\lambda_n = 0$ for j = 1

The unbalanced load at the end of any iteration is given as,

$$\mathbf{R_U^j} = \mathbf{R_E^n} + \Delta\lambda_n \mathbf{R_{ref}} - \mathbf{R_I^j} \qquad (61)$$

With the newly computed unbalanced loads, the unbalanced energy increment is computed as,

$$E_U = \left(\mathbf{R_U^j}\right)^T \Delta\mathbf{r}^j \qquad (62)$$

If the energy increment falls below the convergence criterion, the iteration is stopped and the next displacement increment is applied. If the convergence criterion is not satisfied, next iteration is started with the present unbalanced load.

3. Validation of MATLAB finite element (FE) codes

3.1. Validation of corotational truss FE codes

For the purpose of validation of the developed codes for corotational truss element, a von Mises truss (Figure 4 Vasios 2015) is taken, whose non-dimensional load displacement equilibrium equation is derived in closed form.

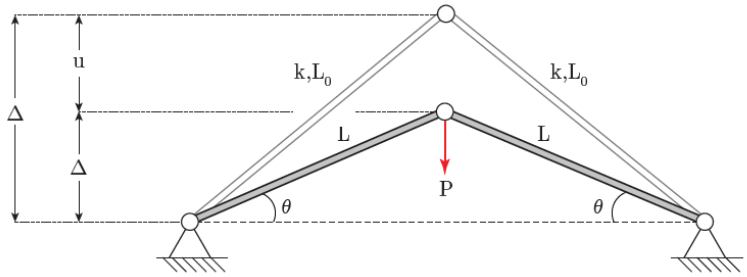

Figure 4: Deformed and undeformed geometry of von Mises truss (Vasios 2015)

The internal forces of the members in the deformed geometry are shown in Figure 5 (Vasios 2015).

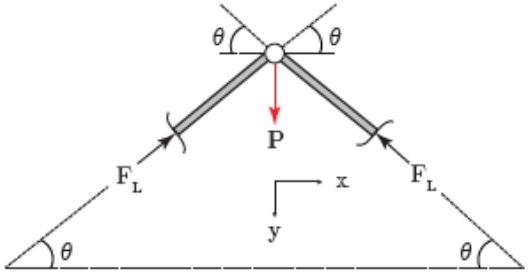

Figure 5: Internal forces in the von Mises truss members (Vasios 2015)

From the equilibrium of the top joint in the deformed configuration, the externally applied force is related to the internal forces of the member as,

$$P = 2F_L \sin\theta \qquad (63)$$

The material constitutive relation is given as,

$$F_L = k(L - L_0) \qquad (64)$$

Considering the compatibility relation from Figure 6 (Vasios 2015), it can be shown that,

$$\frac{L}{L_0} = \sqrt{1 - 2\frac{u}{L_0}\sin\theta_0 + \left(\frac{u}{L_0}\right)^2} \qquad (65)$$

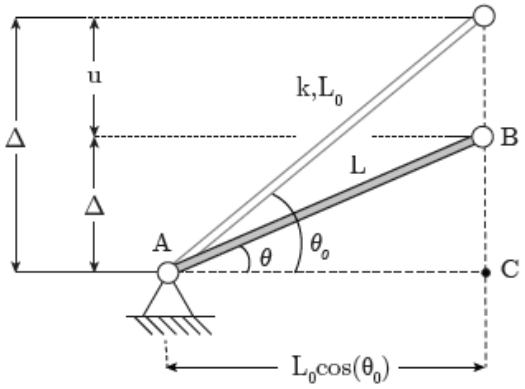

Figure 6: Kinematics of the von Mises truss (Vasios 2015)

Substituting the values of F_L and $\frac{L}{L_0}$, the equilibrium equation 63 becomes,

$$\frac{P}{2kL_0} = \left(\frac{1}{\sqrt{1-2\frac{u}{L_0} sin\,\theta_0 + \left(\frac{u}{L_0}\right)^2}} - 1 \right) \left(sin\,\theta_0 - \frac{u}{L_0} \right) \qquad (66)$$

Defining non-dimensional load λ and non-dimensional displacement a as,

$$\lambda = \frac{P}{2kL_0} \qquad (67)$$

$$a = \frac{u}{L_0} \qquad (68)$$

The non-dimensional equilibrium equation can be written as,

$$\lambda = \left(\frac{1}{\sqrt{1-2a\,sin\,\theta_0 + a^2}} - 1 \right) (sin\,\theta_0 - a) \qquad (69)$$

The results obtained from the developed code for this system taking $\theta_0 = \frac{\pi}{3}$ as well from the analytical solution are shown in Figure 7. It can be seen the result are in good agreement with analytical solution.

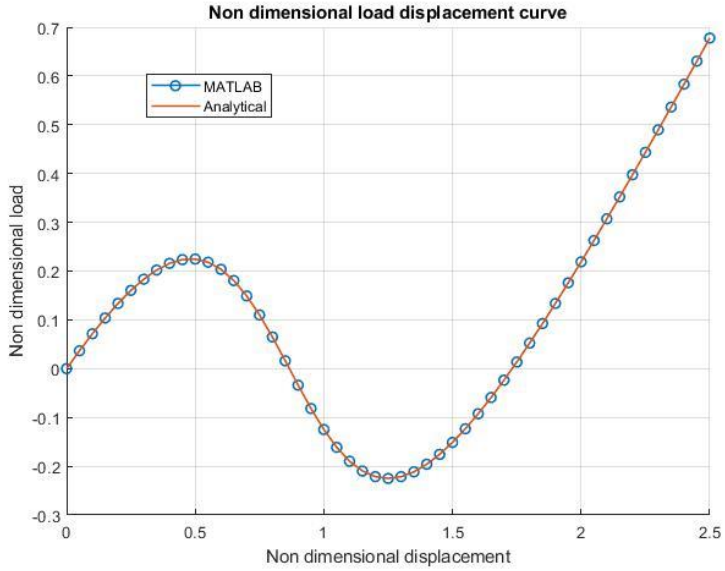

Figure 7: Validation of corotational truss FE codes

3.2. Validation of corotational beam FE codes

For the validation of the corotational beam FE codes, a frame model known as Lee's frame is taken as shown in Figure 8 (Yaw 2009). The column is discretized with 8 elements of equal length while the beam is discretized with 2 equal length elements on the left and 6 equal length elements on the right of the applied load.

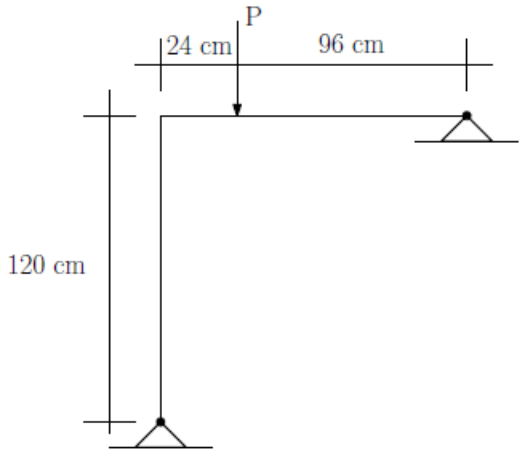

Figure 8: Geometry and loading of Lee's frame (Yaw 2009)

The load displacement behaviour of this structure includes both snap-back and snap-through phenomena (Figure 9). However, a displacement-controlled algorithm can only capture the snap-through phenomenon and not snap-back. For capturing both snap-through and snap-back phenomena, generalized algorithms like arc length method are required. As the present study focuses on snap-through type problem, the load displacement curve of the Lee's frame is validated up to the point where there is a reversal of the displacement at the point of application of the load.

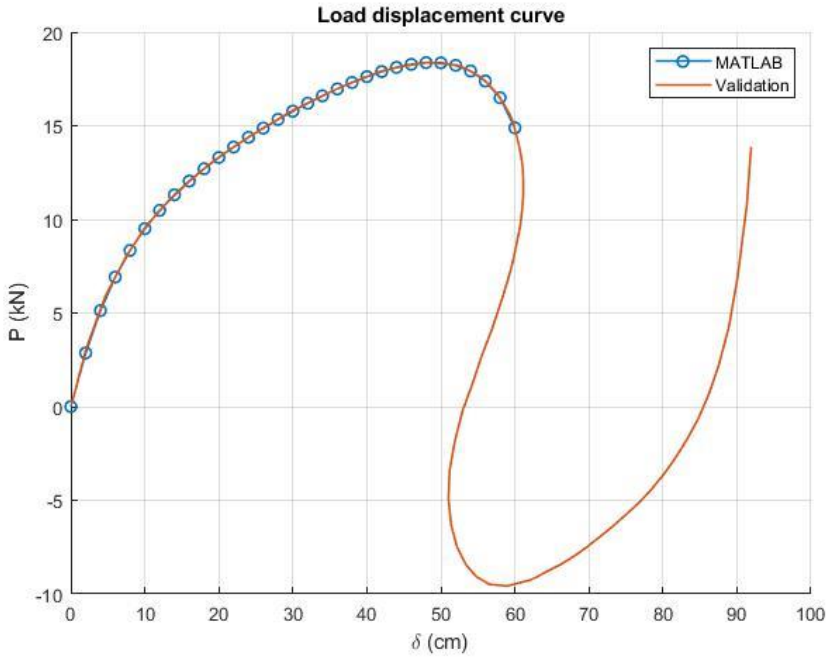

Figure 9: Validation of corotational beam FE codes

From the load displacement curve in Figure 9, it can be seen that the results from the developed MATLAB code are in agreement with that from the results presented in Yaw 2009, till a reversal of the displacement occurs. Beyond about displacement of 61.15 cm, the presently adopted displacement-controlled algorithm will fail to trace the equilibrium path of the system because of the

nature of the solution. For validating, a displacement increment of 2 cm is taken at each step. The deformed geometry of the structure at the applied final displacement value is shown in Figure 10.

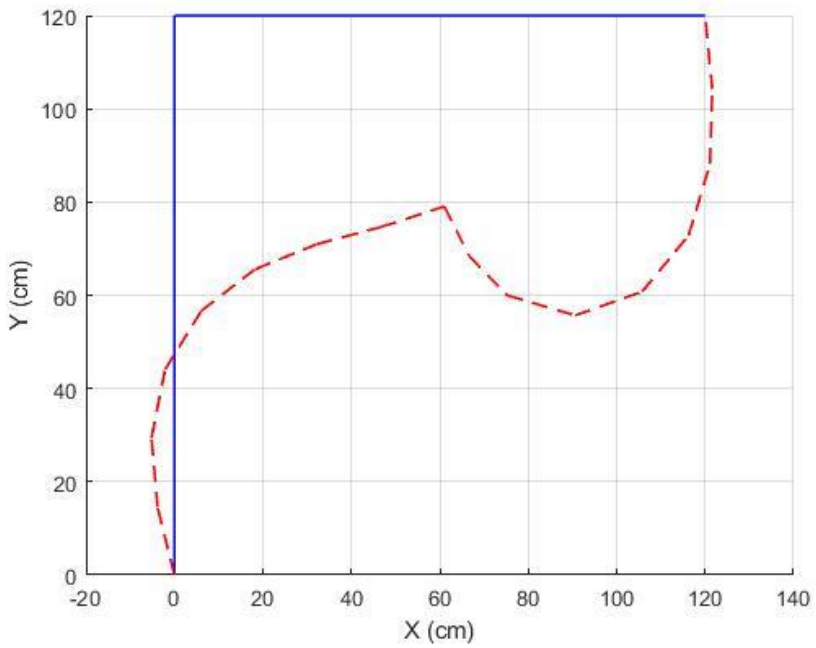

Figure 10: Deformed geometry of the Lee's frame at the applied final displacement

4. Modelling of thin shallow arch

4.1. Theoretical background

Xenidis et al. 2013 proposed the idea of modelling a thin shallow arch by a number of truss elements. A model of shallow arch with transverse loading is shown in Figure 11 (Xenidis et al. 2013).

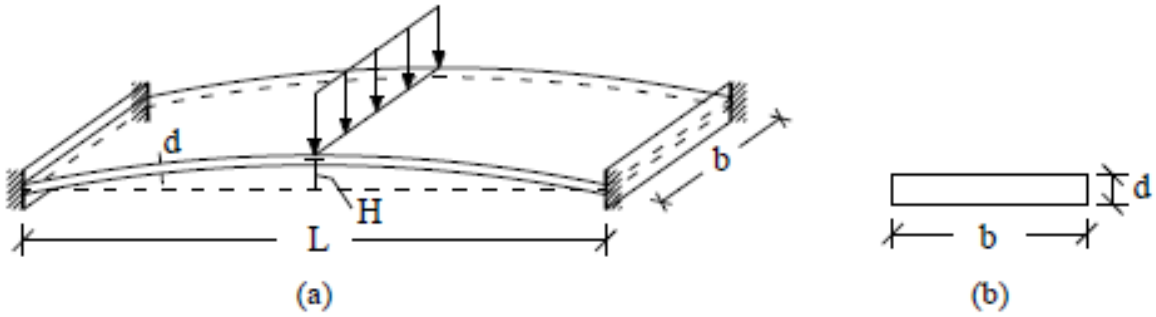

Figure 11: A thin shallow arch model with loading (Xenidis et al. 2013)

The arch is discretized into a network of trusses comprising of 4 sides and 2 diagonals as constituent elements. Since a very shallow arch is taken, the quadrilateral networks are all assumed to be rectangular and equal in dimensions. A schematic of the discretization is shown in Figure 12 (Xenidis et al. 2013). The cross-section properties of the truss elements are obtained by comparison of the stress strain behaviour of an arch element with the stress strain behaviour of the discretized model with truss element as illustrated in Figure 13 (Xenidis et al. 2013).

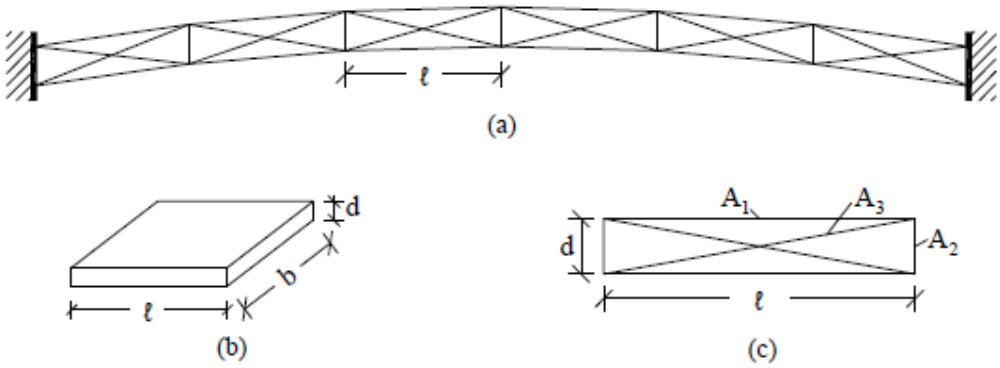

Figure 12: Adopted discretization technique for a thin shallow arch model (Xenidis et al. 2013)

The cross-section properties of the longitudinal bars are found by considering the bending action of an arch element and the deformation in truss elements.

From Figure 13a, $I = \frac{bd^3}{12}$ *(70)* and $\Delta\phi = \frac{Ml}{EI} = \frac{12Ml}{Ebd^3}$ *(71)*

From Figure 13b, $\Delta l = \frac{Nl}{EA_1} = \frac{(M/d)l}{EA_1}$ *(72)* and $\Delta\phi = \frac{2\Delta l}{d} = \frac{2Ml}{EA_1 d^2}$ *(73)*

Comparing both the equations in $\Delta\phi$, area of the longitudinal bars is given as,

$$A_1 = \frac{bd}{6} \qquad (74)$$

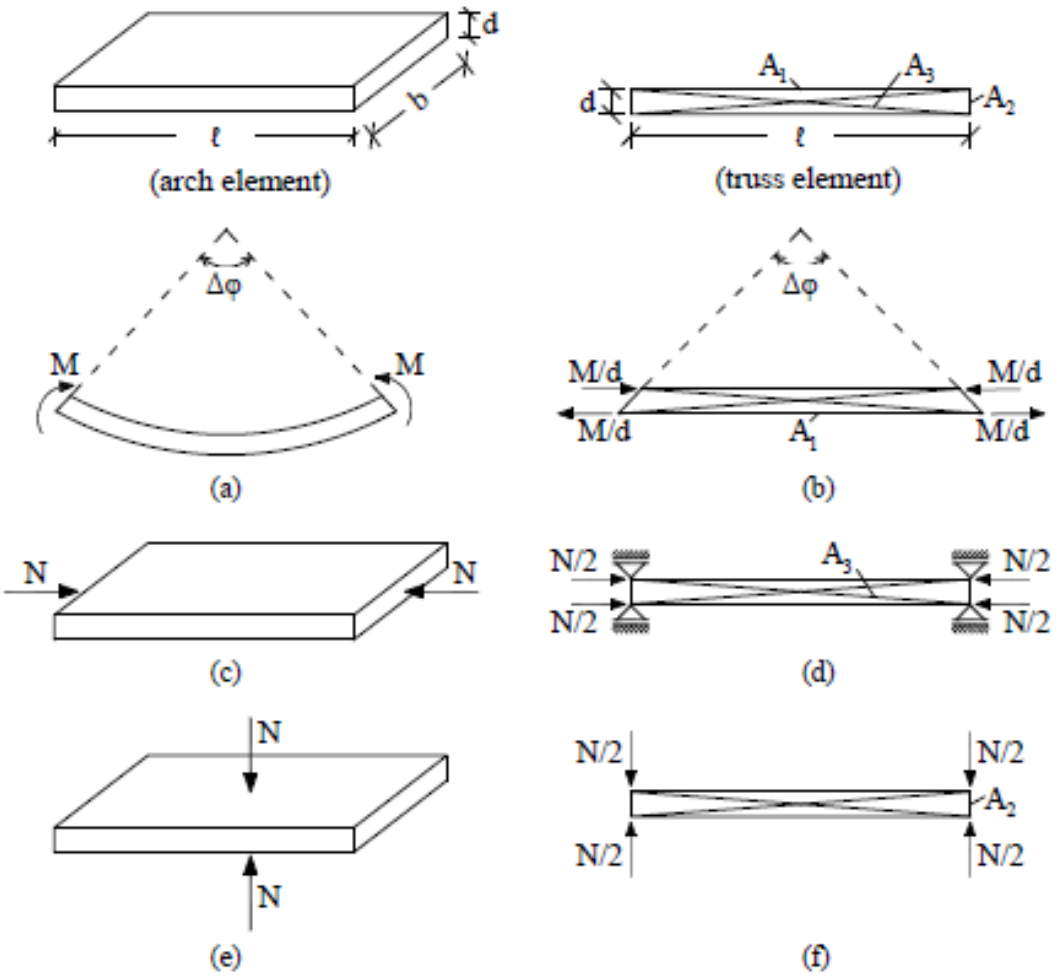

Figure 13: Load deflection behaviour of arch and truss discretized model (Xenidis et al. 2013)

The cross-section properties of the diagonal bars are found by taking into consideration the behaviour in longitudinal direction.

From Figure 13c, $\Delta l = \frac{Nl}{Ebd}$ *(75)*

From Figure 13d, $\Delta l = \frac{(N/2)l}{E(A_3+bd/6)}$ *(76)*

Comparing both the equations, area of the diagonal bars is given as,

$$A_3 = \frac{bd}{3} \qquad (77)$$

The cross-section properties of the transverse elements are found from the consideration of the behaviour in the transverse direction from both the systems.

From Figure 13e, $\Delta d = \frac{Nd}{Ebl}$ *(78)*

From Figure 13f, $\Delta d = \frac{(N/2)d}{EA_2}$ *(79)*

Comparing the equations, area of the transverse bars is given as,

$$A_2 = \frac{bl}{2} \qquad (80)$$

4.2. Numerical modelling

4.2.1. Modelling with truss elements

For the present study, the arch model with parameters presented in Figure 14 (Xenidis et al. 2013) is taken for numerical analysis. The equation of the thin shallow arch is given by,

$$y = H\left(1 - \frac{4x^2}{L^2}\right) \qquad (81)$$

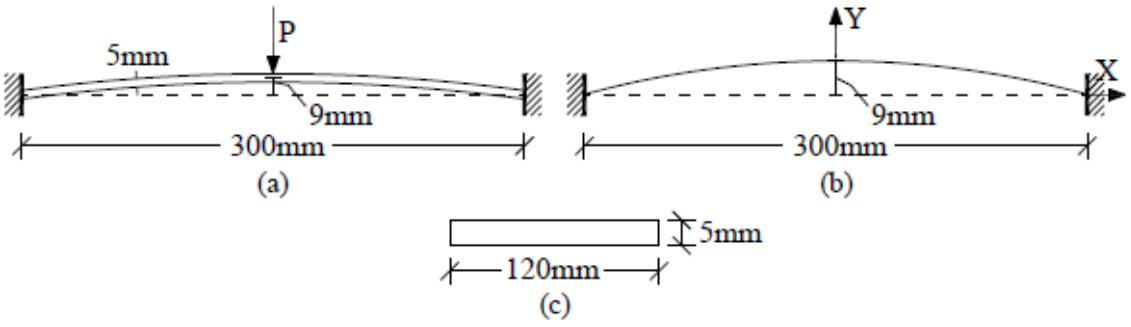

Figure 14: Thin shallow arch model adopted for FEA (Xenidis et al. 2013)

The truss model corresponding to the arch is obtained by discretizing the geometry into 6 rectangular truss networks along the span as given in Figure 12a (Xenidis et al. 2013). The truss elements are modelled using corotational FE approach and a Newton-Raphson iteration is carried out till structural convergence with maximum 10 iterations. The model parameters are given below in SI units.

H = mid height of the arch at mid span = 0.009 m

L = span of the arch = 0.3 m

d = thickness of the arch = 0.005 m

b = width of the arch perpendicular to the paper = 0.120 m

E = Young's modulus of the material = $2*10^{11}$ Pa

l = length of one truss network along the span = L/6 = 0.05 m

A1 = area of longitudinal bars = bd/6 = 10^{-4} m^2

A2 = area of transverse bars = bl/2 = $3*10^{-3}$ m^2

A3 = area of diagonal bars = bd/3 = $2*10^{-4}$ m^2

The model can be imagined as a little less than a 1-foot steel scale with a width of 120 mm and thickness of 5 mm with fixed boundary condition at the ends.

The top node at the mid span of the discretized truss model is given a displacement from 0 m to 0.016 m with an increment of 0.00004 m. The 4 nodes at both ends of the structure are taken as fixed in all the DOFs. The load displacement graph of the model as obtained from the MATLAB code and Xenidis et al. 2013 are presented in Figure 15.

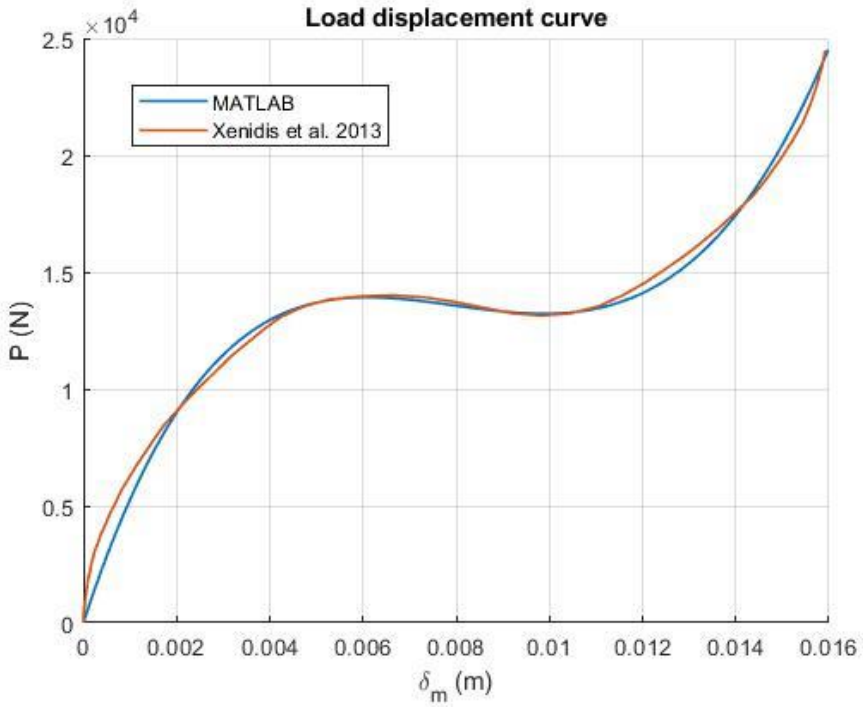

Figure 15: Comparison of truss discretized FE results with Xenidis et al. 2013

The final deformed geometry of the structure is shown in Figure 16.

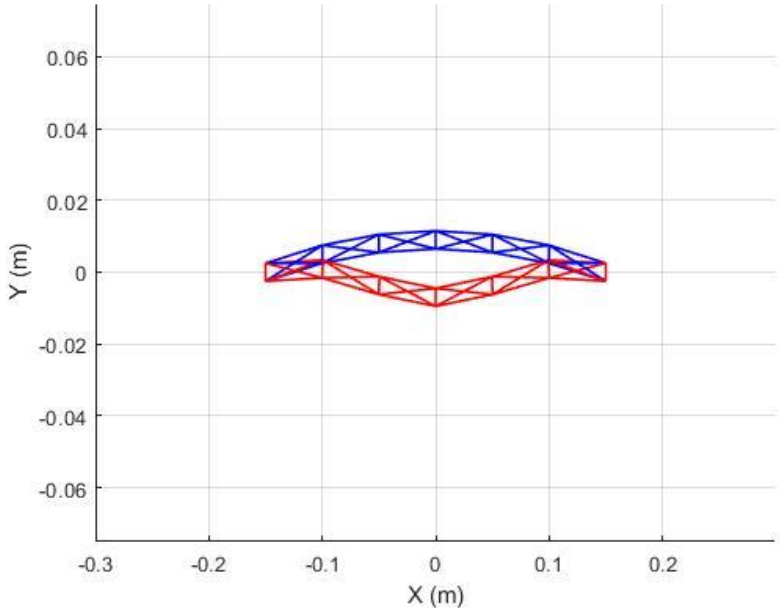

Figure 16: Final deformed geometry of the truss discretized model

4.2.2. Modelling with beam elements

The same model is also studied separately in this project using corotational beam elements. For this purpose, the arch is discretized into a number straight corotational beam elements inclined at different angles with the global coordinate system. The cross-section properties of the beam elements are taken same as that of the arch. Fixity is assumed at the structure ends. The discretized model is subjected to the same displacement history and displacement increment as the case with truss elements.

For the beam elements, the cross-section properties taken are given below.

A = area of the cross section = bd = $6*10^{-4}$ m^2

I = second of inertia = $bd^3/12 = 1.25*10^{-9}$ m^4

Results of the model with varying number of elements are taken for convergence check (Figure 17). It can be seen that the results are converged with 20 elements.

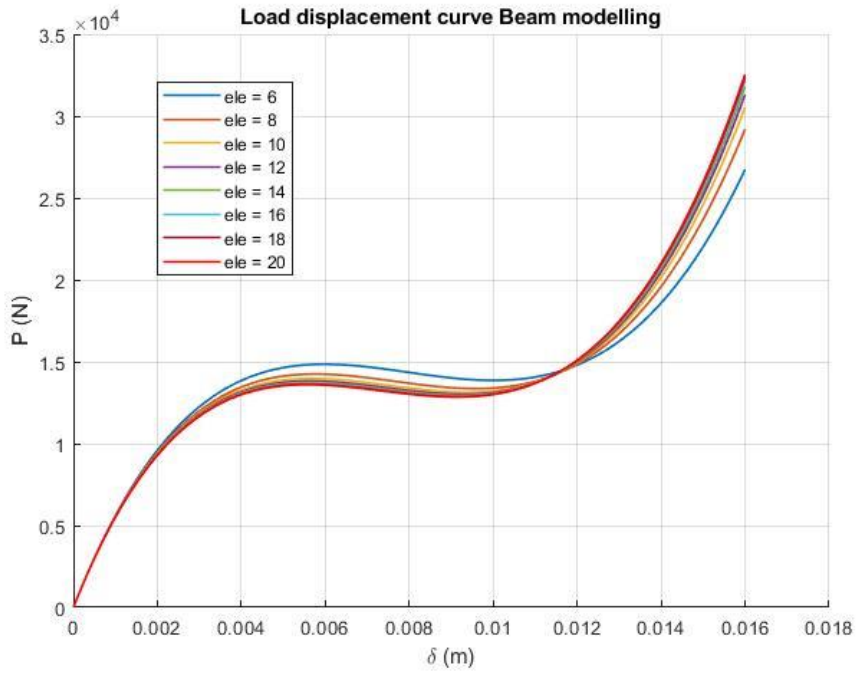

Figure 17: Convergence study of beam discretized model with different number of elements

The final deflected shape of the structure with 20 elements under a top deflection of 0.016 m is shown in Figure 18.

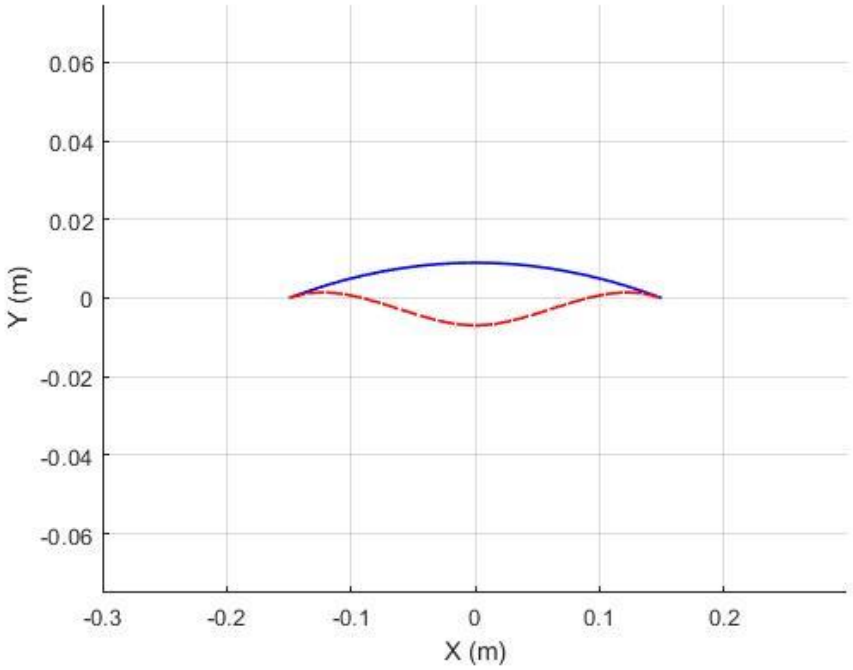

Figure 18: Final deformed geometry of the beam discretized model

The load-displacement curve from the corotational truss formulation with 6 divisions along the span, the result presented in Xenidis et al. 2013 and the result obtained using corotational beam formulation with 20 elements are compiled in Figure 19 for comparison.

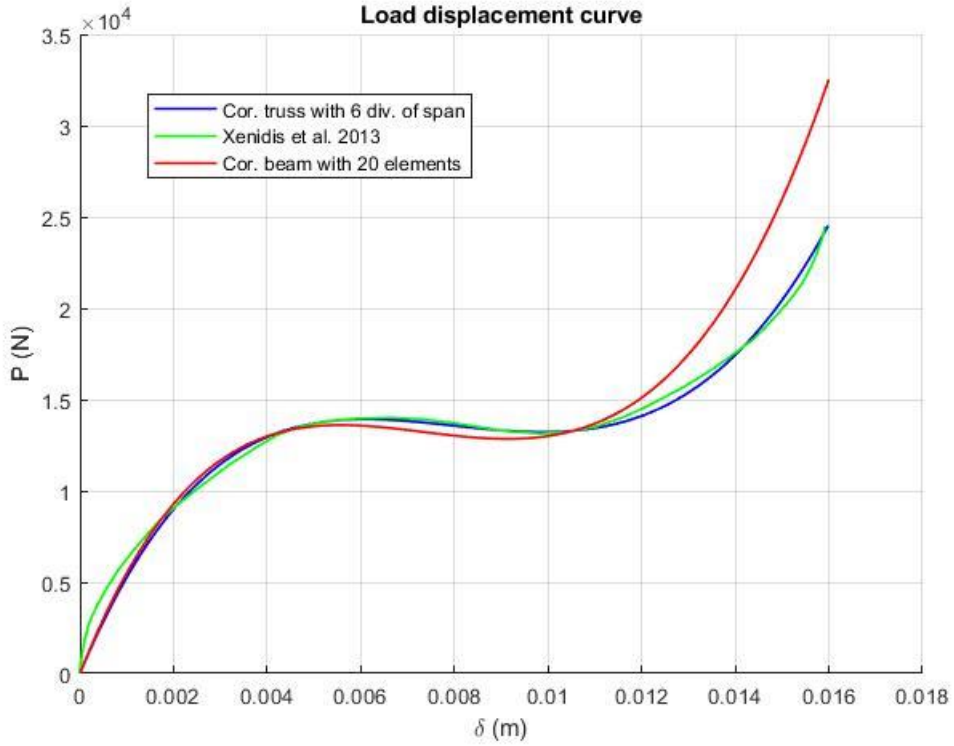

Figure 19: Comparison of beam and truss discretized FE model results with Xenidis et al. 2013

5. Discussion and conclusion

From Figure 19, it can be seen that the result from the discretized corotational truss analysis using developed MATLAB codes for this project is in close agreement with that presented in Xenidis et al. 2013. However, there are some differences in the two results. There could be a number of reasons for the minor differences. In the referenced paper, an iterative solution technique with a fixed number of iterations has been used with the unbalanced force being carried over to the next displacement step as compared to the Newton-Raphson iteration adopted in the developed code with a convergence criterion and no carry over of unbalanced load to next step. Also, in the referenced paper, a displacement control algorithm with elimination of the restrained DOFs from the structural equations is not followed. The method adopted by Xenidis et al. 2013 is similar to a FE analysis with a single point constraint along with penalty approach where the restrained DOFs are substituted with very large values in the system stiffness matrix. Nevertheless, the agreement between the results seems reasonably good despite some differences in the adopted solutions technique.

In the analysis of thin shallow arch under a transverse point load, the phenomenon of snap-through is exhibited in the present study as expected. Due to the presence of snap-through, the structure takes two different paths in a load-controlled analysis while loading and unloading. The critical load at which the snap-through occurs in the truss discretized geometry while loading is found to be P_{cr} = 13.92 kN whereas the critical load at which the structure snaps-through while unloading is P_{cr} = 13.22 kN. The corresponding values for the beam discretized geometry are found to be P_{cr} = 13.6 kN for loading and P_{cr} = 12.85 kN while unloading. The values are comparable in both cases indicating that a truss discretized model can be used as a good approximation for the actual structure for obtaining critical loads.

It can be seen that the load displacement behaviour of both truss and beam discretization are in close agreement for low values of displacement. As the displacement increases, the poorly discretized truss model with only 6 divisions along the span is unable to capture correctly the highly nonlinear force displacement behaviour arising due to geometric nonlinearities. As a consequence, the beam discretized geometry predicts larger value of forces as compared to truss discretized geometry. However, if the arch is shallow, the critical load for the snap-through to occur can be expected to occur for low values of displacements.

Therefore, the idea of discretization of a thin shallow arch subjected to transverse loading by a few networks of trusses whose cross-sectional properties are a function of the cross-section properties of the arch element gives fairly good approximation for estimating the critical behaviour rather than going for a full-fledged finite element analysis using shell elements.

6. References

Xenidis, H., Morfidis, K., Papadopoulos, P.G., 2013. Nonlinear analysis of thin shallow arches subject to snap-through using truss models. Structural Engineering and Mechanics, Vol. 45, No. 4, 521-542.

de Borst, R., Crisfield, M.A., Remmers, J.J.C., Verhoosel, C.V., 2012. Non-linear Finite Element Analysis of Solids and Structures, Second Edition. John Wiley & Sons Ltd.

Ramm, E., 1981. Strategies for Tracing the Nonlinear Response Near Limit Points. Universitat Stuttgart, Germany.

Vasios, N., 2015. Nonlinear Analysis of Structures – The Arc Length Method: Formulation, Implementation and Applications. Harvard University.

Yaw, L.L., 2009. 2D Corotational Beam Formulation. Walla Walla University.

Yaw, L.L., 2009. 2D Corotational Truss Formulation. Walla Walla University.